



## An open-accessed inventory of landslides triggered by the $M_S$ 6.8 Luding earthquake, China on September 5, 2022



Yuandong Huang <sup>a,b,c</sup>, Chenchen Xie <sup>a,b,d</sup>, Tao Li <sup>a,b</sup>, Chong Xu <sup>a,b,\*</sup>, Xiangli He <sup>a,b</sup>, Xiaoyi Shao <sup>a,b</sup>, Xiwei Xu <sup>a,b</sup>, Tao Zhan <sup>e</sup>, Zhaoning Chen <sup>a,b,f</sup>

<sup>a</sup> National Institute of Natural Hazards, Ministry of Emergency Management of China, Beijing, 100085, China

<sup>b</sup> Key Laboratory of Compound and Chained Natural Hazards Dynamics, Ministry of Emergency Management of China, Beijing, 100085, China

<sup>c</sup> China University of Geosciences (Beijing), Beijing, 100083, China

<sup>d</sup> Institute of Disaster Prevention, Sanhe, 065201, China

<sup>e</sup> 107 Geological Team, Chongqing Bureau of Geology and Minerals Exploration, Chongqing, 401120, China

<sup>f</sup> School of Emergency Management Science and Engineering, University of Chinese Academy of Sciences, Beijing, 100049, China

### ARTICLE INFO

#### Keywords:

Luding earthquake  
Landslide inventory  
Coseismic landslides  
Visual interpretation  
Field investigation

### ABSTRACT

This study constructs a preliminary inventory of landslides triggered by the  $M_S$  6.8 Luding earthquake based on field investigation and human-computer interaction visual interpretation on optical satellite images. The results show that this earthquake triggered at least 5 007 landslides, with a total landslide area of 17.36 km<sup>2</sup>, of which the smallest landslide area is 65 m<sup>2</sup> and the largest landslide area reaches 120 747 m<sup>2</sup>, with an average landslide area of about 3 500 m<sup>2</sup>. The obtained landslides are concentrated in the IX intensity zone and the northeast side of the seismogenic fault, and the area density and point density of landslides are 13.8%, and 35.73 km<sup>-2</sup> peaks with 2 km as the search radius. It should be noted that the number of landslides obtained in this paper will be lower than the actual situation because some areas are covered by clouds and there are no available post-earthquake remote sensing images. Based on the available post-earthquake remote sensing images, the number of landslides triggered by this earthquake is roughly estimated to be up to 10 000. This study can be used to support further research on the distribution pattern and risk evaluation of the coseismic landslides in the region, and the prevention and control of landslide hazards in the seismic area.

### 1. Introduction

Strong-magnitude earthquakes often trigger a large number of landslides, which are usually widely distributed, numerous and highly destructive (Fan et al., 2019). In the mountainous areas of southwest China, landslide hazards are very serious due to frequent earthquakes (Shao and Xu, 2022a). The most typical event is the 2008 Wenchuan earthquake, which triggered about 20,000 landslides with a total area of 1 160 km<sup>2</sup> (Dai et al., 2011; Xu et al. 2012a, 2014b). In addition, the 2010 Yushu earthquake (Xu et al., 2012b; Xu et al. 2013; Xu and Xu, 2014a), the 2013 Lushan earthquake (Xu et al., 2015a; Xu et al., 2015b; Ma and Xu, 2019), and the 2014 Ludian earthquake (Tian et al., 2017;

Wu et al., 2020). In the past five years, seismic activity in the southwest has become more frequent, and the impact of coseismic landslides has intensified. For example, the 2017 Jiuzhaigou earthquake (Zhao et al., 2018; Tian et al., 2019; Chen, 2020), the 2019 Changning earthquake (Huang et al., 2021), the 2022 Lushan earthquake (Zhao et al., 2022), the 2022 Maerkang earthquake (Shao et al., 2022). Research on coseismic landslides is still a hot area in the field of natural hazards research (Xu and Xu, 2021). In this context, an efficient and accurate co-seismic landslide inventory after an earthquake plays an important role in supporting disaster prevention and emergency management (Ma et al., 2021; Huang et al., 2022).

On September 5, 2022, an earthquake of  $M_S$  6.8 occurred in Luding

\* Corresponding author. National Institute of Natural Hazards, Ministry of Emergency Management of China, Beijing, 100085, China.  
E-mail address: [chongxu@ninhm.ac.cn](mailto:chongxu@ninhm.ac.cn) (C. Xu).



Production and Hosting by Elsevier on behalf of KeAi

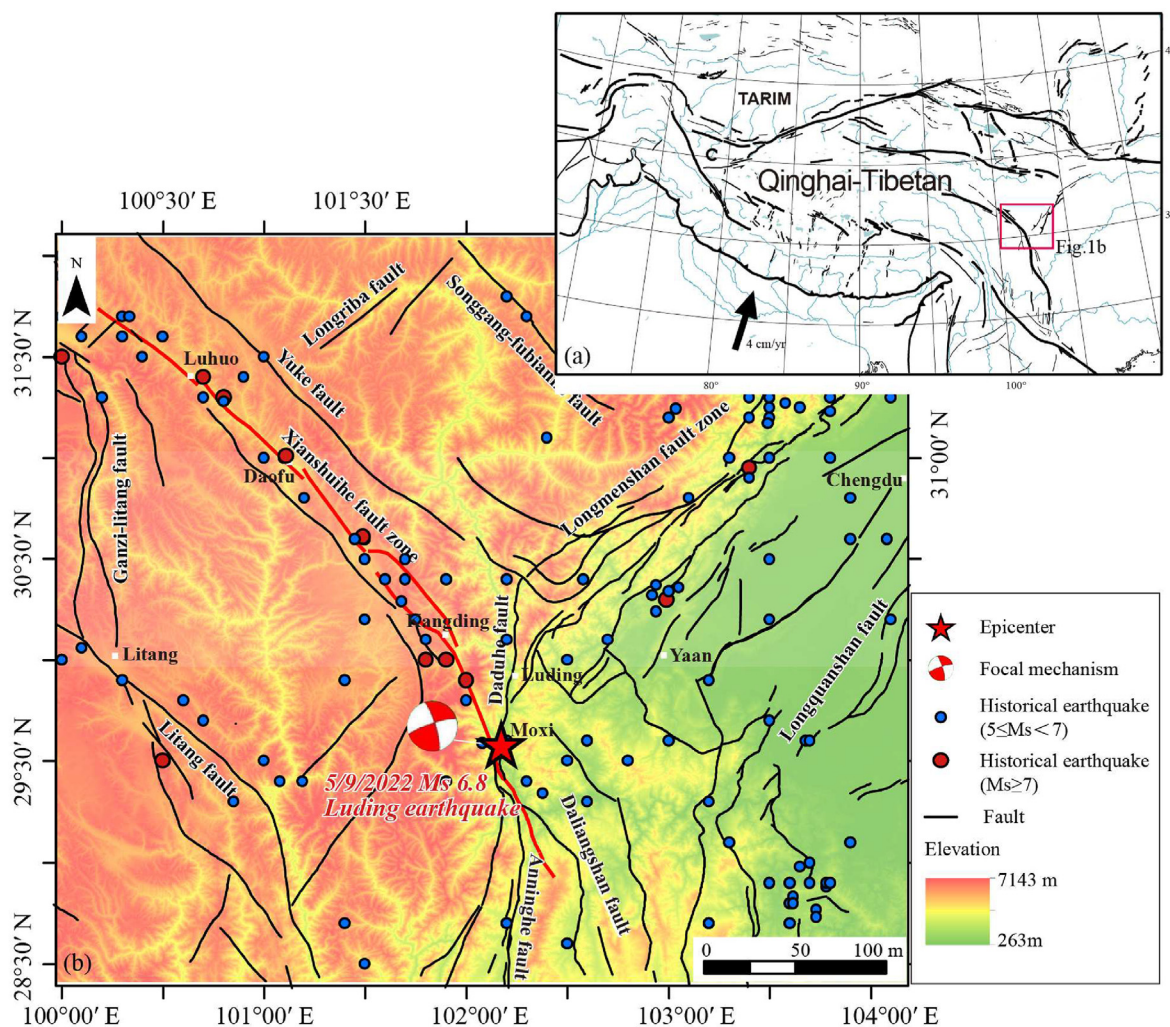


**Fig. 1.** Regional tectonic background and history earthquakes distribution of the September 5, 2022,  $M_s$  6.8 Luding earthquake. (a) A sketch of the tectonic background of the Qinghai-Tibetan Plateau and adjacent areas. (b) Regional tectonic background and history earthquakes distribution map.

County, Ganzi Prefecture, Sichuan Province ( $39.25^{\circ}\text{N}$ ,  $102.08^{\circ}\text{E}$ ), with a depth of 16 km and a maximum intensity of IX degrees ([www.ceic.ac.cn](http://www.ceic.ac.cn)). After the earthquake, several researchers quickly investigated the coseismic landslides, among which Wang et al. (2022) compiled the distribution of coseismic landslides by intelligent extraction of UAV aerial photos and optical satellite images, coupled with deep learning for landslide prediction. Fan et al. (2022) conducted a spatial distribution pattern analysis of geological hazards on this basis. The existing studies have, to some extent, satisfied the timeliness of the co-seismic landslide data, but its accuracy is to be enhanced. To date, a detailed and precise inventory of co-seismic landslides is still lacking.

Therefore, this study aims to establish a detailed inventory of coseismic landslides after this earthquake event. Our study will contribute to further analysis of this event to understand the causes of landslides triggered by this earthquake event and to provide new data to support disaster prevention in the region.

## 2. Geological background of the study area

The seismic area is in the Hengduan Mountains on the southeastern edge of the Qinghai-Tibetan Plateau, a typical alpine valley landscape, the Dadu River runs through the area from north to south, and the river has a large drop. The epicenter of the earthquake is located in the Gongga Mountain, Hailuogou Glacier Forest Park, which is 7 556 m in elevation and has an elevation drop of 6 570 m. The stratigraphic lithology in the

area is mainly Early Sinian granite, Tertiary monzogranite, Permian Leikoupo group dolomite, etc. Due to the long-term strong tectonic and weathering effects, the rock and soil bodies are broken, which provides favorable conditions for the occurrence of geological hazards (Li et al., 2022).

The earthquake occurred near the Moxi fault in the southeastern section of the Xianshuihe faults Zone on the southeastern edge of the Qinghai-Tibetan Plateau. The Xianshuihe faults zone is one of the highly active and large-scale boundary slip fractures regulating the relative motion and extrusion of subplates against the background of the continuous south-eastward extrusion of crustal materials from the southeastern margin of the Qinghai-Tibetan Plateau due to the convergence of the Indo-Eurasian plates (Tapponnir and Molnar, 1977; Tapponnier et al., 2000, 2001; Tapponnier et al., 2001) (Fig. 1). It is located at the boundary between the Bayankela block and the Sichuan-Yunnan block on the eastern edge of the Qinghai-Tibetan Plateau, and intersects with the Longmenshan faults zone and the Anninghe Faults Zone to form the famous "Y-shaped" fracture zone in the western part of Sichuan (Wang et al., 2015). The Xianshuihe faults zone, together with the northwest-oriented Ganzi fault, Yushu fault, Batang fault and Dangjiang fault, south-oriented Anninghe fault, Zemuhe fault and Xiaojiang fault, forms a huge left-slip fault system (Xianshuihe faults System), forming the eastern boundary of the Sichuan-Yunnan rhombic block, spanning 1400 km (Kato et al., 2007; Wen et al., 1989; Allen et al. al., 1991; Wang, 1998; Wang and Burchfiel, 2000; Zhou et al., 2001). The

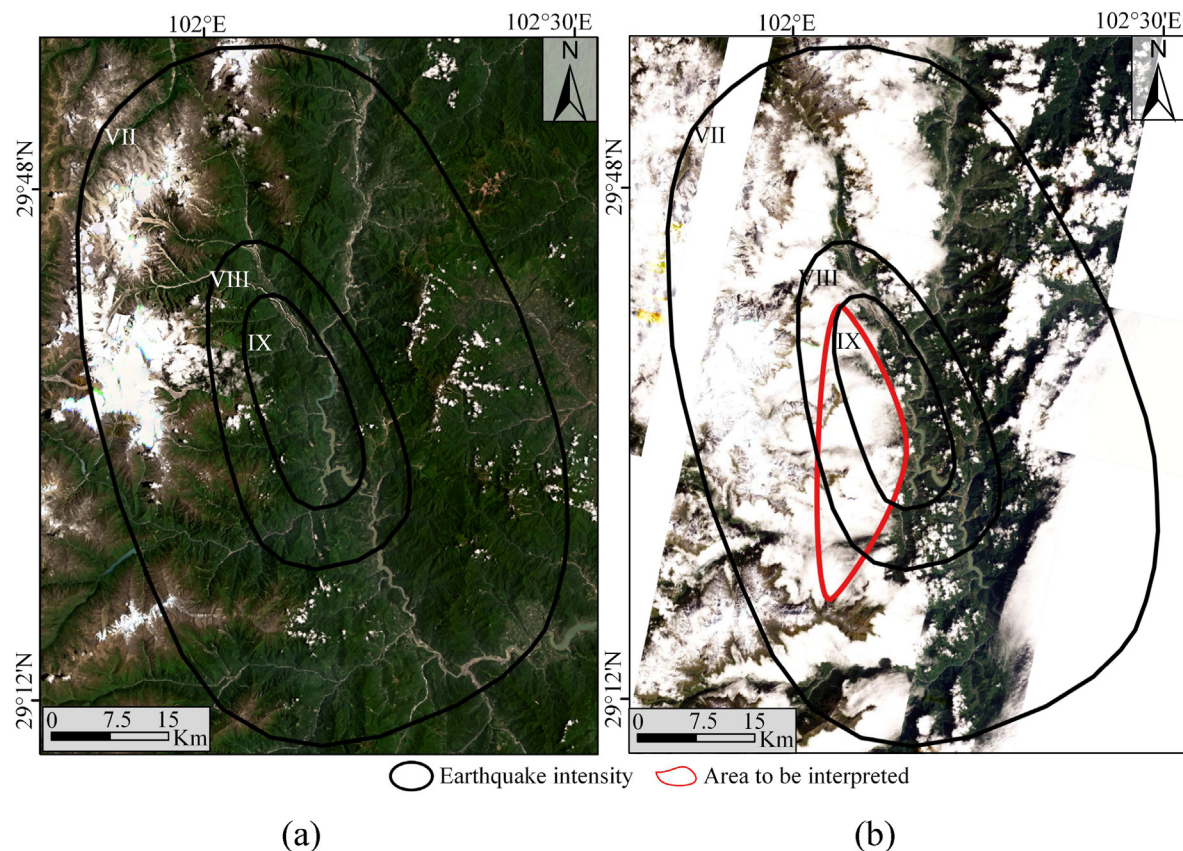


**Fig. 2.** Images of the study area pre- and post-earthquake. (a) July 2022 (b) September 29, 2022.

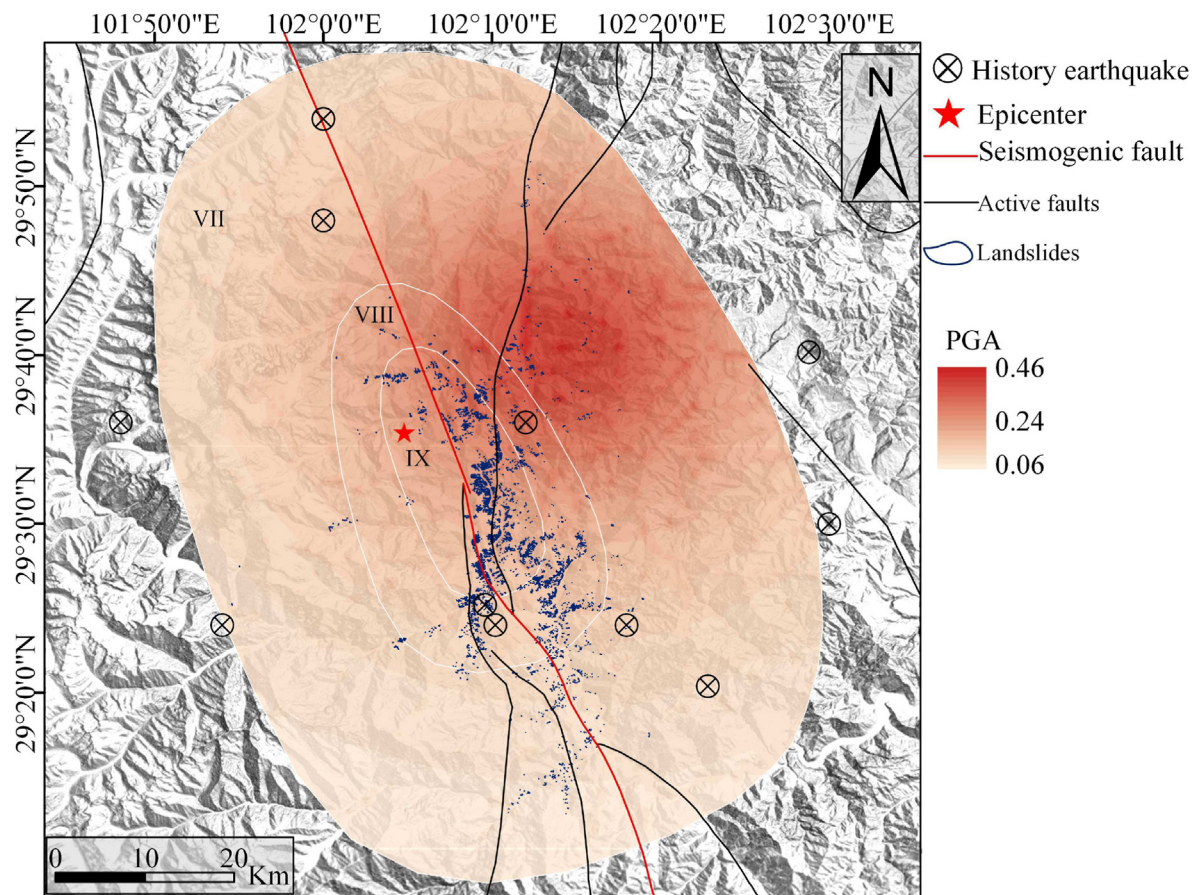


**Fig. 3.** Co-seismic landslides distribution map.

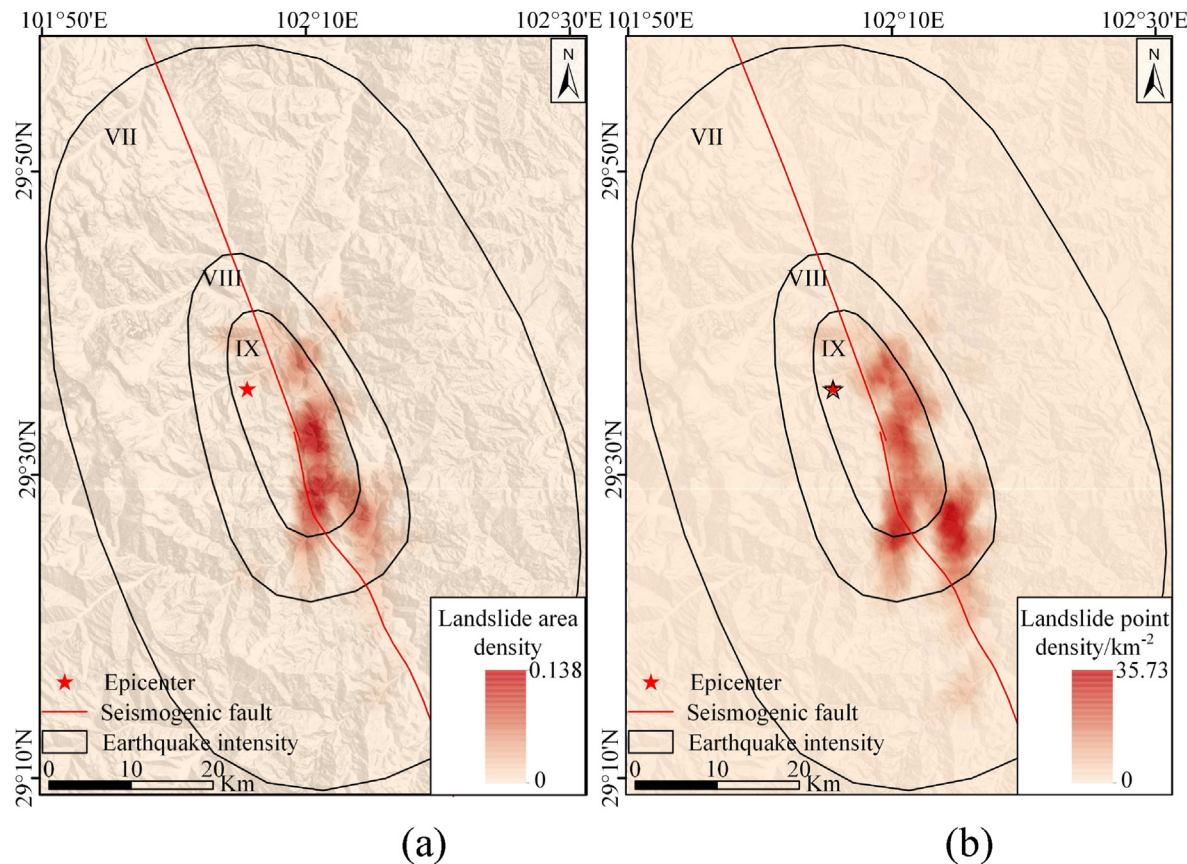


**Fig. 4.** Landslide area and point density maps. (a) landslide area density map, (b) landslide point density map.

Xianshuihe faults zone is 350 km long, starting from the north in the area of the northwest of Donggu and extending to the south of Moxi. The north-west section can be divided into the Luhuo section, the Daofu section and the Qianning section from north-west to south-east, with a strike of about 130°–148°N, and an overall northeast trend, with a south-west trending fracture locally visible (Tang et al., 1984; Allen et al., 1991; Bai et al., 2021). The south-eastern section from Huiyuansi to Kangding consists of four branching faults, the Yalahe fault, the Selaha fault, the Mugecunan fault, and the Zeduotang fault, with an overall strike of about 145° (Pan et al., 2020). The section continues southward near Kangding and joins with the Moxi fault, which has a strike of about 160°, until near Moxi town (Wen et al., 1989; Allen et al., 1991). Zheng et al. (2017) concluded that the Xianshuihe fault exhibited 9 mm/yr of left-rotation displacement and 1–3 mm/yr of positive slip to accommodate the clockwise rotation of the Qinghai-Tibetan Plateau at the Himalayan tectonic junction to southern China. Bai et al. (2022) concluded that the average Late Quaternary slip rate of the Xianshuihe faults system gradually increases from the northwest Ganzi fault to the southeast.

### 3. Data and methods

In this study, all landslide data are extracted from manual visual interpretation. Our work requires more time and input cost than the automatic extraction means based on deep learning. However, the results obtained from visual interpretation are more objective in terms of data accuracy. Our selected remote sensing image is Planet satellite data with a resolution of 3 m. The pre-earthquake image is a global monthly-scale composite image of July and August, 2022, of which the July image is better, while the post-earthquake image is taken from the remote sensing image of the disaster area with an imaging time of September 29, 2022 (Fig. 2).

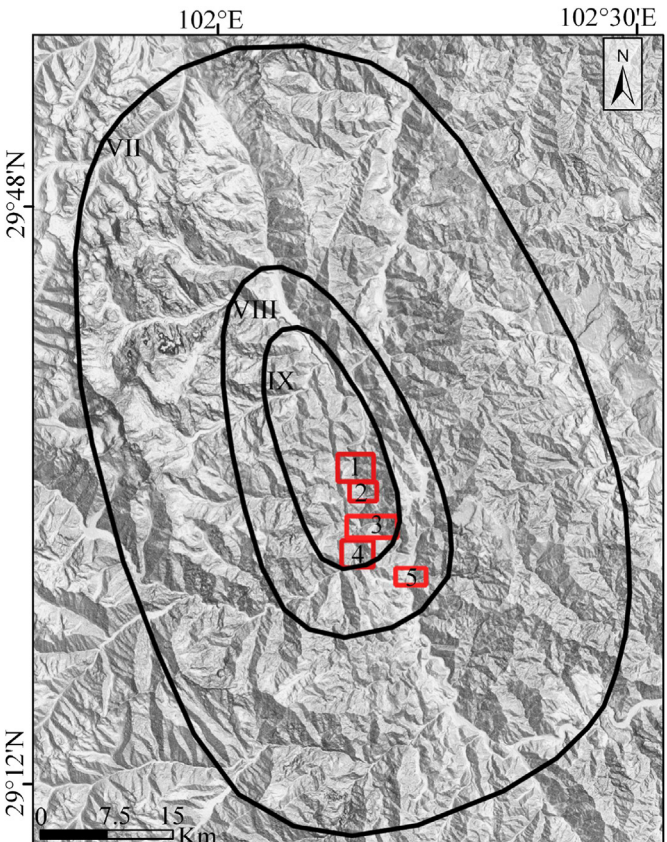


**Fig. 5.** Location map of landslide high-density display area.

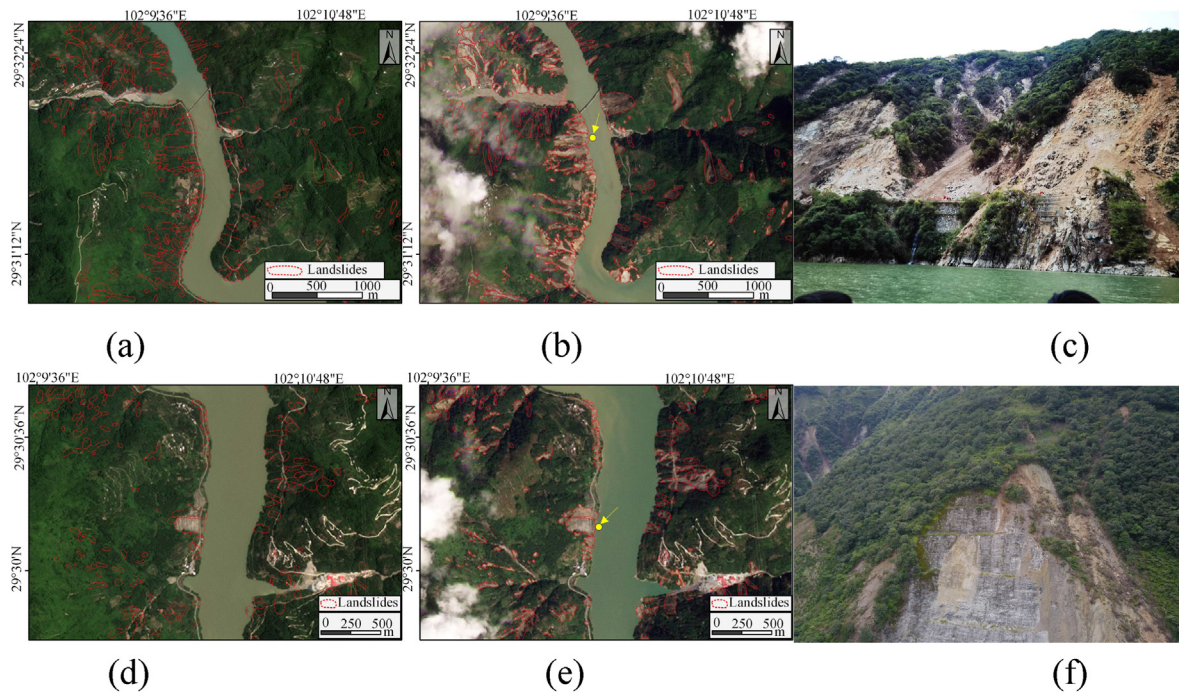


Fig. 6. Landslide high-density areas-1 and 2.

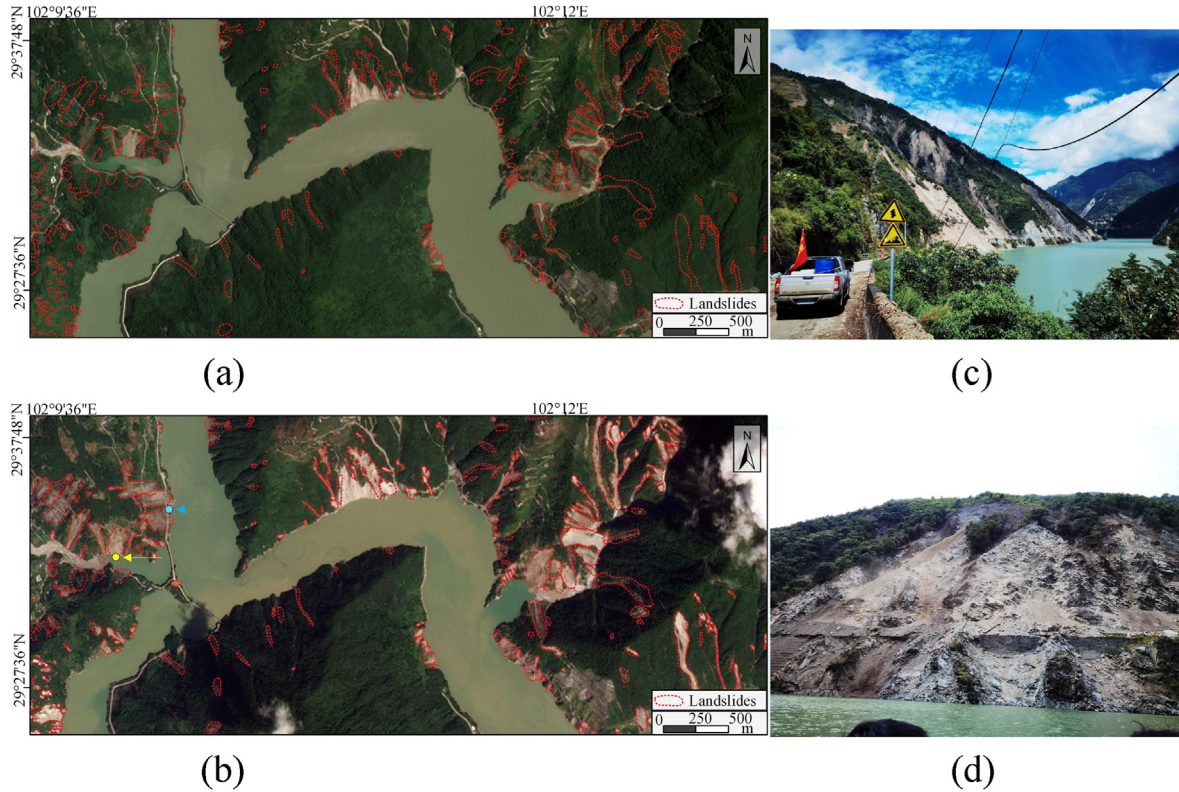
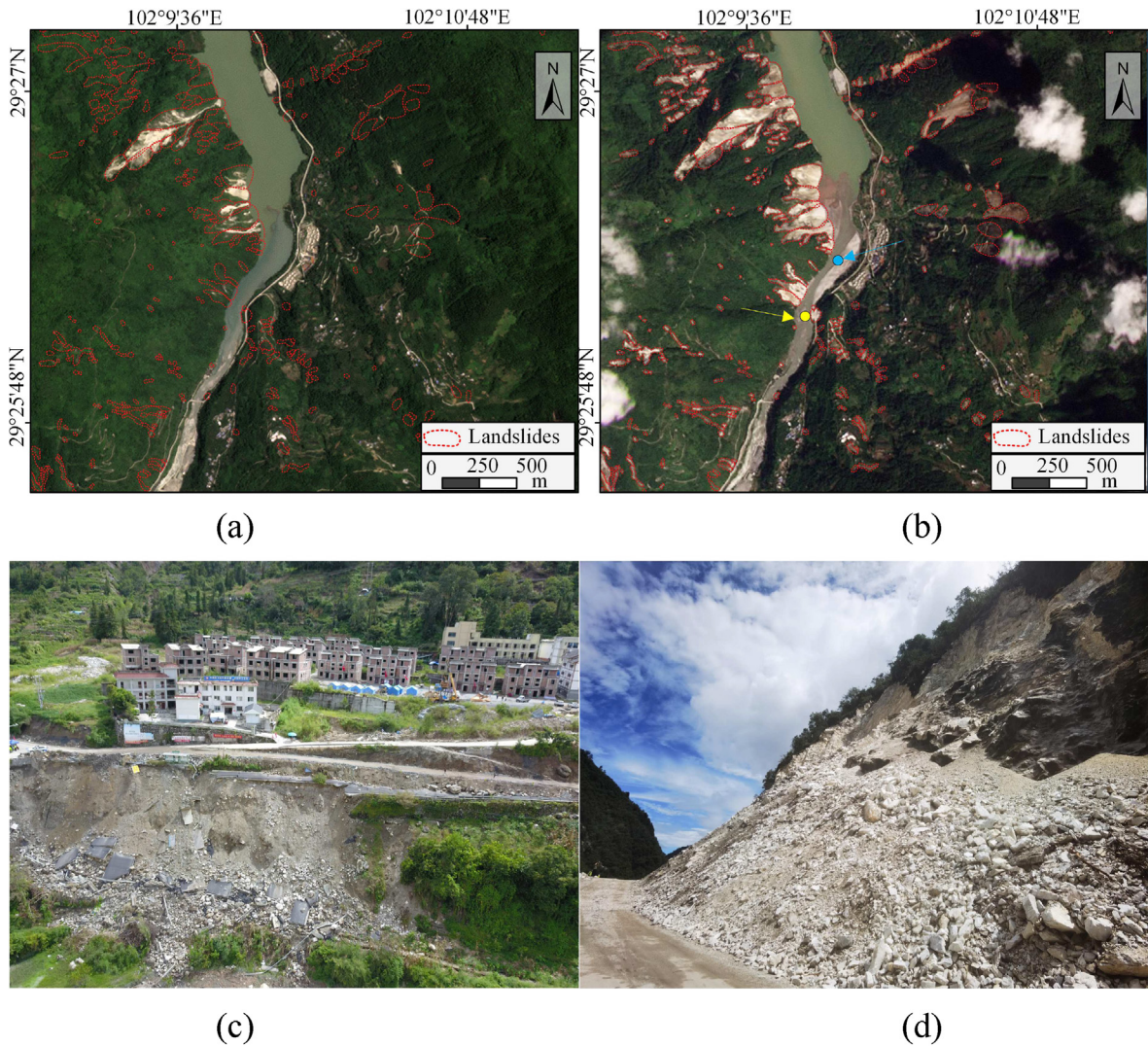


Fig. 7. Landslide high-density areas-3.

The red ranges in Fig. 2(b) mark the areas in our current study for which detailed interpretation has not yet been carried out. This is unavoidable due to the very heavy cloud cover of the images within one month after the earthquake, for which better imaging satellite images are not yet available (Li et al., 2022). Despite the presence of fuzzy areas, the clearer remote sensing image range in Fig. 2(b) covers most of the seismic intensity IX and VIII zones, which highly overlaps with the landslide

probability high occurrence zone obtained by Wang et al. (2022) based on the co-seismic landslide prediction model, and thus this image data is sufficient to support our study.

On the GIS platform, we interpreted remote sensing images, mainly utilizing image comparison before and after the earthquake and identifying features such as landslide geometrical shape and hue for comprehensive determination. Secondly, we conducted a field survey of the



**Fig. 8.** Landslide high-density areas-4.

affected area, photographed and recorded typical landslides, and compared the satellite images with the field photos to enhance the accuracy of the interpreted signs. In addition, we used ALOS 12.5m DEM data (<https://search.asf.alaska.edu/>) to create a 3D view to ensure that we were more accurate when circling the landslide area. In summary, we have adopted several effective means to ensure that the results obtained in this study are reliable, objective, and of significant value.

#### 4. Results

##### 4.1. Inventory of coseismic landslides

In this study, visual interpretation was performed for the seismic intensity VII degree zone and above, and a total of 5 007 landslides were obtained, with a total landslide area of  $17.36 \text{ km}^2$ , of which the smallest landslide area was  $65 \text{ m}^2$  and the largest landslide area reached  $120\,747 \text{ m}^2$ , with an average landslide area of  $3\,466.78 \text{ m}^2$ . The distribution is shown in Fig. 3, and the preliminary analysis of the spatial distribution shows that the landslides are concentrated in the seismic intensity VIII and IX zones. The PGA data are obtained from the USGS website (<https://earthquake.usgs.gov/>), and the distribution of PGA has some deviation from the intensity distribution published by the China Earthquake Administration. This may be because the PGA map published by USGS is mainly based on computational simulation means, lacking the

support of field surveys and abundant station records, and the results have some deviation from the actual situation. The seismogenic faults and landslide distribution have obvious connections, and the distribution of coseismic landslides is concentrated on both sides of the seismogenic faults, and the number of landslides on the northeast side is more than that on the southwest side.

To further study the distribution concentration trend of landslides, we conducted a density analysis of the area and number of landslides and considering a large number of landslides in the study area, we searched with a radius of 2 km. The results are shown in Fig. 4. The highest landslide area density is 13.8%, and the high-density area is mainly concentrated in the intensity IX-degree zone and the northeast side of the seismogenic fault. The highest value of landslide point density is  $35.73 \text{ km}^{-2}$ , similar to the distribution pattern of area density, and the high-density area is also concentrated in the IX-degree zone and the northeast side of the seismogenic fault.

##### 4.2. High-density area

Based on the above study, we selected five areas with a high-density of landslide distribution for demonstration. The locations of these five areas are shown in Fig. 5.

Fig. 6(a) and (b) show the pre- and post-earthquake images of area 1 in Fig. 5, and Fig. 6(c) shows a photograph of the field landslide taken at

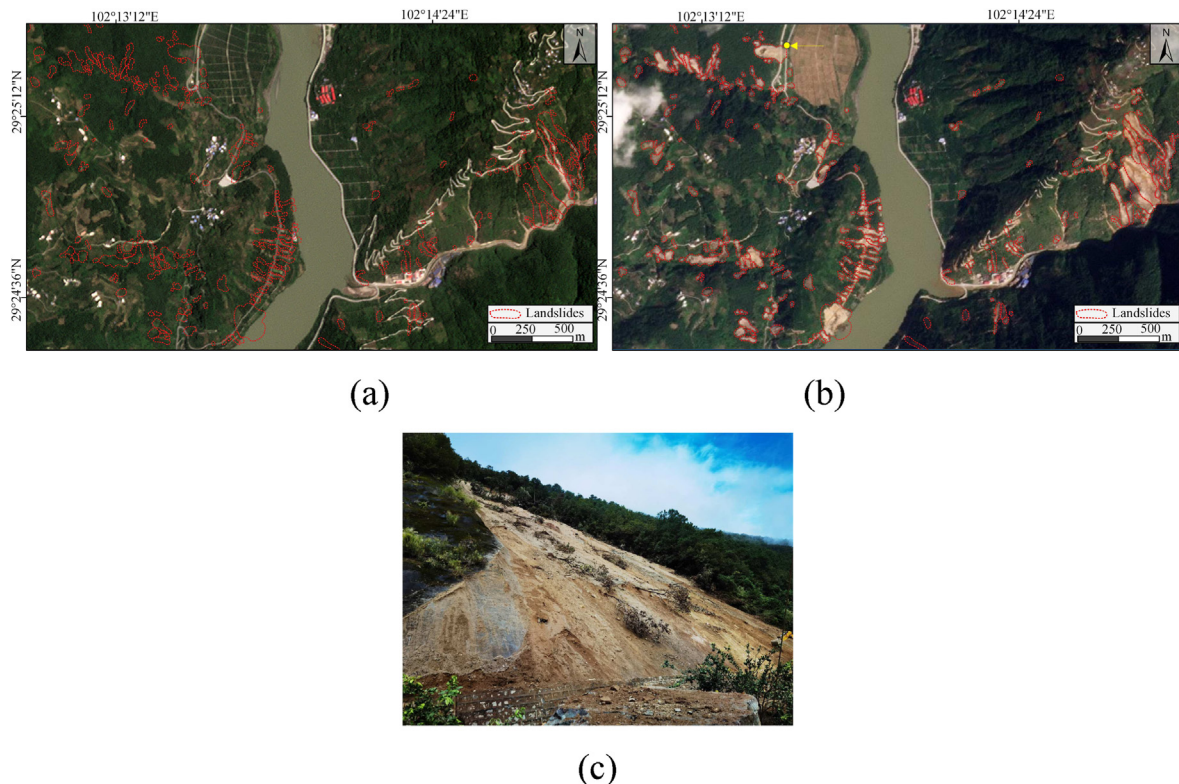


**Fig. 9.** Landslide high-density area-5

the yellow marked point in Fig. 6(b). Fig. 6(d) and (e) show the pre- and post-earthquake images of area 1 in Fig. 5, and Fig. 6(f) shows the field landslide photo taken at the yellow marked point in Fig. 6(e).

**Fig. 7(a) and (b)** show the pre- and post-earthquake images of area 3 in Fig. 5, while **Fig. 7(c) and (d)** show the field landslide photographs taken at the blue and yellow marked points in Fig. 7(b), respectively.

Fig. 8(a) and (b) show the pre- and post-earthquake images of area 4 in Fig. 5, Fig. 8(c) and (d) show the field landslide photographs taken at the blue and yellow marked points in Fig. 8(b), respectively.

**Fig. 9(a) and (b)** show the pre- and post-earthquake images of area 5 in Fig. 5, and **Fig. 9(c)** shows a photograph of the field landslide taken at the yellow marked point in **Fig. 9(b)**.

## 5. Conclusion

In this study, based on Planet satellite images with a resolution of 3 m, the range above the intensity VII degree zone of the 2022  $M_S$  6.8 Luding earthquake was used as the study area to visually interpret the co-seismic landslides triggered by the event. The results showed that in the study area, at least 5 007 co-seismic landslides were distributed, with a total landslide area of  $17.36 \text{ km}^2$ , of which the smallest landslide area was  $65 \text{ m}^2$  and the largest landslide area reached  $120\,747 \text{ m}^2$ , with an average landslide area of  $3\,466.78 \text{ m}^2$ . The landslides were concentrated in the seismic intensity VIII and IX zones. Due to the post-earthquake cloud cover, the areas that could not be fully deciphered were marked in this study, and the database will be improved in the subsequent work.

## **Author agreement**

All the authors who contributed to the study have approved the final version. This is the first submission to this journal and do not consider submitting to other Journals. And we would like to give the permission to the publisher to reproduce this paper in all media.

## **Declaration of competing interest**

The authors declared that they have no conflicts of interest to this work.

### Acknowledgments

This study was supported by the National Natural Science Foundation of China (42077259). We thank Planet Labs PBC. (<https://www.planet.com/>) for free access to satellite images used in this study.

## Appendix A. Supplementary data

Supplementary data associated with this article can be found, in the online version, at <https://doi.org/10.1016/j.eqrea.2022.100181>.

Appendix

The supplementary file includes the epicentre, possible seismogenic fault, VII-degree and above seismic intensity area, area no available post-quake satellite image, and the preliminary inventory of 5 007 landslides in vector format related to the  $M_S$  6.8 Luding earthquake, China on September 5, 2022, which can be freely accessed in the online version.

## References

- Allen, C.R., Luo, Z., Qian, H., Wen, X., Zhou, H., Huang, W., 1991. Field study of a highly active fault zone: the Xianshuhe fault of southwestern China. *Geol. Soc. Am. Bull.* 103 (9), 1178–1199. [https://doi.org/10.1130/0016-7606\(1991\)103<1178:FSOHA>2.3.CO;2](https://doi.org/10.1130/0016-7606(1991)103<1178:FSOHA>2.3.CO;2).

Bai, M., Chevalier, M.L., Leloup, P.H., Li, H., Pan, J., Replumaz, A., Wang, S., Li, K., Wu, Q., Liu, F., 2021. Spatial slip rate distribution along the SE Xianshuhe fault, eastern Tibet, and earthquake hazard assessment. *Tectonics* 40 (11), e2021TC006985. <https://doi.org/10.1029/2021TC006985>.

Bai, M., Chevalier, M.-L., Li, H., Pan, J., Wu, Q., Wang, S., Liu, F., Jiao, L., Zhang, J., Zhang, L., Gong, Z., 2022. Late Quaternary slip rate and earthquake hazard along the

- Qianning segment, Xianshuihe fault. *Acta Geol. Sin.* 46 (7), 2312–2332. <https://doi.org/10.3969/j.issn.0001-5717.2022.07.005>.
- Chen, X.l., Shan, X.j., Wang, M.m., Liu, C.g., Han, N. n., 2020. Distribution pattern of coseismic landslides triggered by the 2017 Jiuzhaigou Ms 7.0 earthquake of China: control of seismic landslide susceptibility. *ISPRS Int. J. Geo-Inf.* 9 (4), 198. <https://doi.org/10.3390/ijgi9040198>.
- Dai, F., Xu, C., Yao, X., Xu, L., Tu, X., Gong, Q.M., 2011. Spatial distribution of landslides triggered by the 2008 Ms 8.0 Wenchuan earthquake, China. *J. Asian Earth Sci.* 40 (4), 883–895. <https://doi.org/10.1016/j.jseas.2010.04.010>.
- Fan, X., Scaringi, G., Korup, O., West, A.J., van Westen, C.J., Tanyas, H., Hovius, N., Hales, T.C., Jibson, R.W., Allstadt, K.E., Zhang, L., Evans, S.G., Xu, C., Li, G., Pei, X., Xu, Q., Huang, R., 2019. Earthquake-induced chains of geological hazards: patterns, mechanisms, and impacts. *Rev. Geophys.* 57 (2), 421–503. <https://doi.org/10.1029/2018RG000626>.
- Fan, X., Wang, X., Dai, L., Fang, C., Deng, Y., Zou, C., Tang, M., Wei, Z., Dou, X., Zhang, J., Yang, F., Chen, L., Wei, T., Yang, Y., Zhang, X., Xia, M., Ni, T., Tang, X., Li, W., Dai, K., Dong, X., Xu, Q., 2022. Characteristics and spatial distribution pattern of Ms 6.8 Luding earthquake occurred on September 5, 2022. *J. Eng. Geol.* In press <http://www.gcdz.org/en/article/id/77d603ac-db72-4aac-822e-f37abe547b9c>.
- Huang, Y., Xu, C., Zhang, X., 2021. Spatial distribution and influence factors of landslides triggered by the 2019 Ms 6.0 Changning, Sichuan, China Ms6. 0 earthquake: a statistical analysis based on QGIS. In: IOP Conference Series: Earth and Environmental Science. IOP Publishing. <https://doi.org/10.1088/1755-1315/861/5/052007>.
- Huang, Y., Xu, C., Zhang, X., Li, L., 2022. Bibliometric analysis of landslide research based on the WOS database. *Nat. Hazards Res.* 2 (2), 49–61. <https://doi.org/10.1016/j.nhres.2022.02.001>.
- Kato, N., Lei, X., Wen, X., 2007. A synthetic seismicity model for the Xianshuihe fault, southwestern China: simulation using a rate-and state-dependent friction law. *Geophys. J. Int.* 169 (1), 286–300. <https://doi.org/10.1111/j.1365-246X.2006.03313.x>.
- Li, W., Chen, J., Lu, H., Shan, Y., Li, Z., Chen, B., Wu, L., Xu, Z., Li, W., Zhang, P., 2022. Emergency analysis of the impact of the luding Ms 6.8 earthquake on Hailuogou Glacier. *Geomatics Inf. Sci. Wuhan Univ.* <https://doi.org/10.13203/j.whugis20220593>.
- Ma, S., Xu, C., 2019. Assessment of co-seismic landslide hazard using the Newmark model and statistical analyses: a case study of the 2013 Lushan, China, Mw6.6 earthquake. *Nat. Hazards* 96 (1), 389–412. <https://doi.org/10.1007/s11069-018-3548-9>.
- Ma, S., Shao, X., Xu, C., He, X., Zhang, P., 2021. MAT.TRIGRS (V1.0): a new open-source tool for predicting spatiotemporal distribution of rainfall-induced landslides. *Nat. Hazards Res.* 1 (4), 161–170. <https://doi.org/10.1016/j.nhres.2021.11.001>.
- Pan, J., Li, H., Chevalier, M.-L., Bai, M., Liu, F., Liu, D., Zheng, Y., Lu, H., Zhao, Z., 2020. A newly discovered active fault on the Selaha-Kangding segment along the SE Xianshuihe fault: the South Mugucus fault. *Acta Geol. Sin.* 94 (11), 3178–3188. <https://doi.org/10.19762/j.cnki.dizhixuebao.2020196>.
- Shao, X., Xu, C., 2022a. Earthquake-induced landslides susceptibility assessment: a review of the state-of-the-art. *Nat. Hazards Res.* <https://doi.org/10.1016/j.nhres.2022.03.002>.
- Shao, X., Xu, C., Wang, P., Li, L., He, X., Chen, Z., Huang, Y., Xu, X., 2022. Two public inventories of landslides induced by the 10 June 2022 Maerkang Earthquake swarm, China and ancient landslides in the affected area. *Nat. Hazards Res.* <https://doi.org/10.1016/j.nhres.2022.09.001>.
- Tang, R., Qian, H., Chang, W., Chang, C., Cao, Y., Liu, S., 1984. On the seismogeological setting and conditions of seismogenic structures of 1981 Daofu earthquake. *Seismol. Geol.* 6 (2), 33–41.
- Tappognier, P., Xu, Z., Roger, F., Meyer, B., Arnaud, N., Wittlinger, G., Yang, J., 2001. Oblique stepwise rise and growth of the Tibet Plateau. *science* 294 (5547), 1671–1677. <https://doi.org/10.1126/science.105978>.
- Tappognier, P., Molnar, P., 1977. Active faulting in a Cenozoic tectonics of China [J]. *J. Geophys. Res.* 82 (2), 2905–2930. <https://doi.org/10.1029/JB082i020p02905>.
- Tian, Y., Xu, C., Chen, J., Hong, H., 2017. Spatial distribution and susceptibility analyses of pre-earthquake and coseismic landslides related to the Ms 6.5 earthquake of 2014 in Ludian, Yunan, China. *Geocarto Int.* 32 (9), 978–989. <https://doi.org/10.1080/10106049.2016.1232316>.
- Tian, Y., Xu, C., Ma, S., Xu, X., Wang, S., Zhang, H., 2019. Inventory and spatial distribution of landslides triggered by the 8th August 2017 Mw 6.5 Jiuzhaigou Earthquake, China. *J. Earth Sci.* 30 (1), 206–217. <https://doi.org/10.1007/s12583-018-0869-2>.
- Wang, E., 1998. Late Cenozoic Xianshuihe-Xiaojiang, Red River, and Dali Fault Systems of Southwestern Sichuan and Central Yunnan. Geological Society of America, China. <https://doi.org/10.1130/SPE327>.
- Wang, E., Burchfiel, B.C., 2000. Late Cenozoic to Holocene deformation in southwestern Sichuan and adjacent Yunnan, China, and its role in formation of the southeastern part of the Tibetan Plateau. *Geol. Soc. Am. Bull.* 112 (3), 413–423. [https://doi.org/10.1130/0016-7606\(2000\)112<413:LCTHDI>2.0.CO;2](https://doi.org/10.1130/0016-7606(2000)112<413:LCTHDI>2.0.CO;2).
- Wang, M., Li, T., Meng, L., 2015. Back analysis of stress field in the intersection region of Y shaped fault, Sichuan. *J. Railw. Sci. Eng.* 12 (5), 1088–1095. <https://doi.org/10.19713/j.cnki.43-1423/u.2015.05.016>.
- Wang, X., Fang, C., Tang, X., Dai, L., Fan, X., Xu, Q., 2022. Research on emergency evaluation of landslides induced by Luding Ms6.8 Earthquake. *Geomatics Inf. Sci. Wuhan Univ.* <https://doi.org/10.13203/j.whugis20220586>.
- Wen, X., Allen, C., Luo, Z., Qian, H., Zhou, H., Huang, W., 1989. Segmentation, geometric features, and their seismotectonic implications for the Holocene Xianshuihe fault zone. *Acta Seismologica Sinica* 11 (11), 362–372.
- Wu, W., Xu, C., Wang, X., Tian, Y., Deng, F., 2020. Landslides triggered by the 3 August 2014 Ludian (China) Mw 6.2 Earthquake: an updated inventory and analysis of their spatial distribution. *J. Earth Sci.* 31 (4), 853–866. <https://doi.org/10.1007/s12583-020-1297-7>.
- Xu, C., Xu, X., Dai, F., Saraf, A.K., 2012a. Comparison of different models for susceptibility mapping of earthquake triggered landslides related with the 2008 Wenchuan earthquake in China. *Comput. Geosci.* 46, 317–329. <https://doi.org/10.1016/j.cageo.2012.01.002>.
- Xu, C., Xu, X., Lee, Y.H., Tan, X., Yu, G., Dai, F., 2012b. The 2010 Yushu earthquake triggered landslide hazard mapping using GIS and weight of evidence modeling. *Environ. Earth Sci.* 66 (6), 1603–1616. <https://doi.org/10.1007/s12665-012-1624-0>.
- Xu, C., Xu, X., Yu, G., 2013. Landslides triggered by slipping-fault-generated earthquake on a plateau: an example of the 14 April 2010, Ms 7.1, Yushu, China earthquake. *Landslides* 10 (4), 421–431. <https://doi.org/10.1007/s10346-012-0340-x>.
- Xu, C., Xu, X., 2014a. Statistical analysis of landslides caused by the Mw 6.9 Yushu, China, earthquake of April 14, 2010. *Nat. Hazards* 72 (2), 871–893. <https://doi.org/10.1007/s11069-014-1038-2>.
- Xu, C., Xu, X., Yao, X., Dai, F., 2014. Three (nearly) complete inventories of landslides triggered by the May 12, 2008 Wenchuan Mw 7.9 earthquake of China and their spatial distribution statistical analysis. *Landslides* 11 (3), 441–461. <https://doi.org/10.1007/s10346-013-0404-6>.
- Xu, C., Xu, X., Shyu, J.B.H., 2015a. Database and spatial distribution of landslides triggered by the Lushan, China Mw 6.6 earthquake of 20 April 2013. *Geomorphology* 248, 77–92. <https://doi.org/10.1016/j.geomorph.2015.07.002>.
- Xu, C., Xu, X., Shyu, J.B.H., Gao, M., Tan, X., Ran, Y., Zheng, W., 2015b. Landslides triggered by the 20 April 2013 Lushan, China, Mw 6.6 earthquake from field investigations and preliminary analyses. *Landslides* 12 (2), 365–385. <https://doi.org/10.1007/s10346-014-0546-1>.
- Xu, X., Xu, C., 2021. Natural Hazards Research: an eternal subject of human survival and development. *Nat. Hazards Res.* 1 (1), 1–3. <https://doi.org/10.1016/j.nhres.2020.12.003>.
- Zhao, B., Wang, Y., Luo, Y., Li, J., Zhang, X., Shen, T., 2018. Landslides and dam damage resulting from the Jiuzhaigou earthquake (8 August 2017), Sichuan, China. *R. Soc. Open Sci.* 5 (3), 171418. <https://doi.org/10.1098/rsos.171418>.
- Zhao, B., Li, W., Su, L., Wang, Y., Wu, H., 2022. Insights into the landslides triggered by the 2022 lushan Ms 6.1 earthquake: spatial distribution and controls. *Rem. Sens.* 14 (17), 4365. <https://doi.org/10.3390/rs14174365>.
- Zheng, G., Wang, H., Wright, T.J., Lou, Y., Zhang, R., Zhang, W., Shi, C., Huang, J., Wei, N., 2017. Crustal deformation in the India-Eurasia collision zone from 25 years of GPS measurements. *J. Geophys. Res. Solid Earth* 122 (11), 9290–9312. <https://doi.org/10.1002/2017JB014465>.
- Zhou, R., He, Y., Huang, Z., Ni, X., Yang, T., 2001. The slip rate and strong earthquake recurrence interval on the Qianning-Kangding segment of the Xianshuihe fault zone. *Acta Seismologica Sinica* 23 (3), 250–261. <https://doi.org/10.3321/j.issn:0253-3782.2001.03.004>.